Experimental Calibration of Bifurcation Superstructure of Nonlinear System

By H. Lin[1] and S. C. S. Yim,[2] Member, ASCE

Abstract: Results of a medium-scale experimental study revealing the underlying superstructure in bifurcation sets of a submerged, moored ocean system are reported. The experimental model, assimilating nonlinear moored structural responses, consists of a spherical buoy and attached multipoint mooring lines. The model is excited under a periodic wave field in a closed channel. Sources of system nonlinearity include complex geometric restoring force and coupled fluid-structure interaction exciting forces. Experimental setup, configuration, and classification of the measured results are described. Characteristic motions observed include harmonic, subharmonic, and ultraharmonic responses. Nonlinear primary and secondary resonances in the response are identified in frequency response diagrams, which also indicate the existence of intricate patterns of the nonlinear global behavior.

INTRODUCTION

Complex response behavior, including nonharmonic responses, instabilities, and sensitivity to initial conditions, has been demonstrated in various numerical and small-scale experimental models [e.g., Moon (1987)]. Recognizing the difficulties in designing large-scale experiments modeling nonlinear system phenomena, a medium-scale experimental investigation in calibrating the analytical predictions about the existence of bifurcation superstructure in nonlinear response is summarized and reported in this note.

The experimental model is to assimilate the nonlinear response of a submerged, moored ocean system subjected to periodic wave excitations. Various nonlinear responses, e.g., subharmonic and ultraharmonic (Gottlieb and Yim 1992) are observed and classified, and their stability regions are defined. Existence of the corresponding superstructure in bifurcations described in the analytical study (Gottlieb et al. 1997) is indicated and inferred. Validity of the analytical model of a symmetric multipoint moored structural system subjected to a deterministic exciting field described by small amplitude waves and weak collinear current is also assessed.

SYSTEMS CONSIDERED

The system considered is a single-degree-of-freedom (surge motion only), hydrodynamically excited, submerged, rigid structure moored by four elastic lines with geometric nonlinearity (Fig. 1). Characteristics of the wave fields are governed by kinematics and return flow of prescribed periodic waves. The complex exciting force includes both coupled fluid-structure interaction drag and inertial terms.

Experimental Setup

Experimental configurations are formulated with the intention of calibrating the various nonlinear phenomena in response behavior predicted by corresponding single-degree-of-freedom analytical models (Gottlieb et al. 1997), including the existence and stability of subharmonics, ultraharmonics (n/m = 1/2, 1/1, 2/1), and the underlying bifurcation superstructure.

The experimental model consists of a spherical rigid body on a rod supported by guyed masts 1.83 m above the bottom of a closed wave channel (Yim et al. 1993). To compare with the predictions by the single-degree-of-freedom analytical model, motions of the sphere are constrained in surge direction only. Two Delrin bearings are placed on the sphere to reduce the friction and minimize the free play between the sphere and the rod. The sphere, made of PVC with diameters of 45.72 cm, is filled with water when submerged. Springs of various stiffness (146 or 292 N/m) are attached to the sphere at an angle of 60° ($b = l_{1,2}/2$ in Fig. 1) or 90° ($b = 0$) to provide a nonlinear restoring force. Note that the linear behavior of the high-tensioned springs is in direct contrast to the complex response of nonlinear, inelastic (hysteretic), and low-tensioned cables examined by Triantafyllou and Yue (1995), where cable properties and sag are the major sources of nonlinearity. The damping mechanism includes a linear-system (structural) component (associated with the system connections and contact points of instrumentation), and a time-dependent coulomb friction component (due to the setup of restricted surge motion). The coulomb friction originates from the lift force (in heave) and combined drag/lift moment (in pitch). The

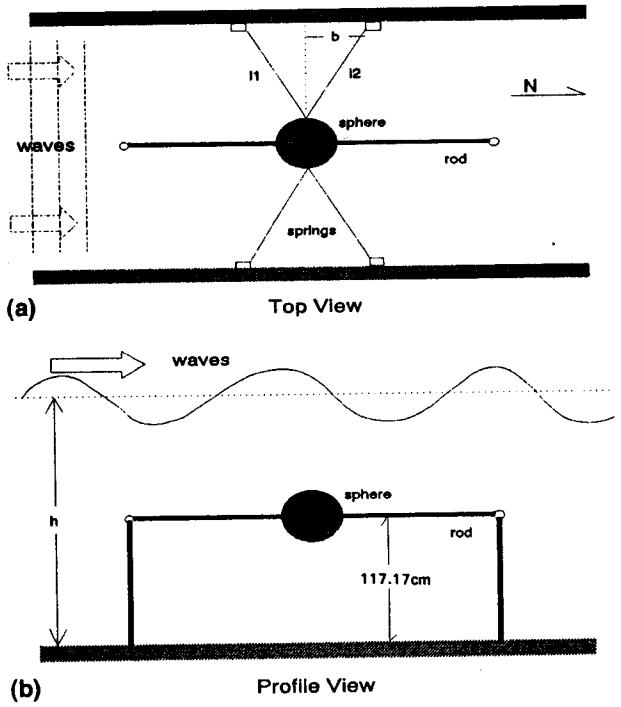

FIG. 1. Experimental Model of Submerged, Hydrodynamically Damped and Excited Nonlinear Ocean Structural System

[1]Res. Assoc., Dept. of Civ. Engrg., Oregon State Univ., Corvallis, OR 97331.

[2]Prof., Dept. of Civ. Engrg., Oregon State Univ., Corvallis, OR.

Note. Associate Editor: Dimitrios Karamanlidis. Discussion open until September 1, 1998. To extend the closing date one month, a written request must be filed with the ASCE Manager of Journals. The manuscript for this technical note was submitted for review and possible publication on April 12, 1996. This technical note is part of the *Journal of Engineering Mechanics*, Vol. 124, No. 4, April, 1998. ©ASCE, ISSN 0733-9399/98/0004-0471–0475/$4.00 + $.50 per page. Technical Note No. 13055.

variability in the friction force is a result of changing amplitude and direction of normal force due to the oscillatory nature of the hydrodynamic drag/lift forces.

Governing Equation

Lumping the time-dependent coulomb friction and structural damping into an equivalent linear system damping coefficient, the equation of motion is

$$M\ddot{x} + C_s\dot{x} + R(x) = F_D(x, \dot{x}) + F_I(\dot{x}, \ddot{x}) \quad (1)$$

where x and $\dot{x}$ = surge displacement and velocity, respectively; M = mass of system; R = nonlinear restoring force; C_s = effective system damping coefficient; and F_D and F_I = drag and inertial components of the exciting force, respectively.

The restoring force includes the effects due to the mooring (R_M) and the hydrostatic buoyancy (R_B). The sphere used for this experiment is virtually neutrally buoyant when submerged. Therefore, the forcing caused by R_B is negligible and not considered here. The restoring force $R(x)$ is then given by

$$R(x) \cong R_M = K\left[4x + l_c\left(2b\frac{l_1 - l_2}{l_1 l_2} - 2x\frac{l_1 + l_2}{l_1 l_2}\right)\right] \quad (2)$$

where K = spring constant (see Fig. 1 for b); $l_{1,2}$ = spring lengths; and l_c = initial spring length.

The exciting force consists of a relative Morison drag (F_D) and an inertial component (F_I)

$$F_D = \frac{\rho}{2} C_D A_P (u - x)|u - \dot{x}| \quad (3a)$$

$$F_I = \rho\forall(1 + C_A)\left[\frac{\partial u}{\partial t} + (u - \dot{x})\frac{\partial u}{\partial x}\right] - \rho\forall C_A\ddot{x} \quad (3b)$$

where C_D = hydrodynamic viscous drag coefficient; C_A = added mass coefficient; A_P = projected drag area; $\forall$ = displaced volume; and u = fluid particle velocity.

EXPERIMENTAL FACILITIES

The experiment is conducted at the O. H. Hinsdale Wave Laboratory at Oregon State University in a two-dimensional wave channel. The flume is 104.24 m long, 3.66 m wide, and 4.57 m deep. Waves are generated by a hydraulically driven, hinged flap wave board, and a VAX 3400 server and two VAX 3100 stations with optical communication links for wave generation control and 64 channels of digital are used for data acquisition.

Data recorded in 14 channels during each test include wave profiles at several locations along the channel, currents, sphere displacements, and tensions in the springs. The recorded data are conditioned, filtered, and stored on the VAX 3400.

The wave profiles are measured by six resistive type wave gauges. The horizontal and vertical velocities of the water particles are measured by MINILAB model SD-12 current meters. The displacements of the sphere are measured by UniMeasure model P-75A string pots. Strain gauges are placed on the lines connecting the springs to the sphere to measure the components of the restoring force. The initial (static) value of the spring tension can be adjusted by tightening or loosening the springs from the carriage above. Two underwater cameras provide a second means of measuring the sphere displacements. The cameras also provide visualization of the displacements of the sphere.

Three wave gauges are placed on each side of the model at distances of 0.46, 1.22, and 3.35 m from the model. The current meter is placed 25.40 cm upstream of the model, 55.88 cm from the side wall, at a depth of 22.86 cm. Two string pots are attached to the sphere for displacement measurements on opposite sides to offset the force placed on the sphere by the string pots. String pots are also placed on the springs to measure their elongations, which are used to determine the restoring forces.

EXPERIMENTAL RESULTS

Continuous Search Tests

Four search test runs are performed with the 60° and 90° configurations. In the continuous search mode, the wave frequencies are normally changed by 0.01 Hz every 2–3 min. Excitation parameters (frequencies and amplitudes) are manually recorded and used in data acquisition tests to further examine the interesting nonlinear phenomena observed.

The first and second search tests are conducted with the 60° configuration. In the first search test, the wave height is kept constant at 0.27 m and the frequency is increased from 0.41 to 0.70 Hz with an increment of 0.01 Hz. The response amplitude steadily decreases as the frequency increases.

In the second search test, the frequency is decreased from 0.70 to 0.13 Hz with a decrement of 0.01 Hz, and the wave height is increased from 0.37 to 0.64 m in going from 0.70 to 0.45 Hz. The response amplitude increases as the wave height increases and frequency decreases. The search tests are designed to identify specific nonlinear phenomena, which can be more frequently observed in large amplitude responses. However, to prevent the response from becoming too large and damaging the test model, the maximum response amplitude is maintained at about 0.92 m by adjusting the wave height as necessary when the frequency is varied.

The third and fourth search tests are conducted with the 90° configuration. For this geometric configuration, nonlinear behavior can be achieved at a much lower amplitude. In the third search test, the excitation frequency is first increased from 0.10 to 1.00 Hz and then decreased from 1.00 to 0.10 Hz. During this test ultraharmonic responses are observed from 0.15 to 0.18 Hz and period doublings are observed from 0.46 to 0.56 Hz. Ultraharmonic responses are also observed from 0.14 to 0.12 Hz and a possible transition point from ultraharmonic to subharmonic response is observed at 0.11 Hz.

The fourth search test is intended to further investigate the nonlinear phenomena observed previously. For instance, the transition near 0.11 Hz from ultraharmonic to subharmonic observed in the third search test is examined to pinpoint the bifurcation point. However, steady-state responses observed are strictly ultraharmonic with no identifiable transition region. The disappearing of the transition may be due to the response sensitivity to initial conditions and excitation variations.

Based on the experimental results, the characteristic frequency responses with the 60° and 90° configurations are shown in Figs. 2(a) and 2(b), respectively. As noted previously, to maintain the sphere response sufficiently large for nonlinear behavior without damaging the model, wave amplitude and frequency need to be maneuvered accordingly at the same time. The nonlinear relationship between response and excitation in a three-parameter space can be interpreted by plotting amplitude ratio (response amplitude/wave amplitude) against excitation frequency instead of a standard frequency response curve (Nayfeh and Mook 1979). Resonances and nonlinear relationships between the system response and the excitation are fully revealed in Fig. 2.

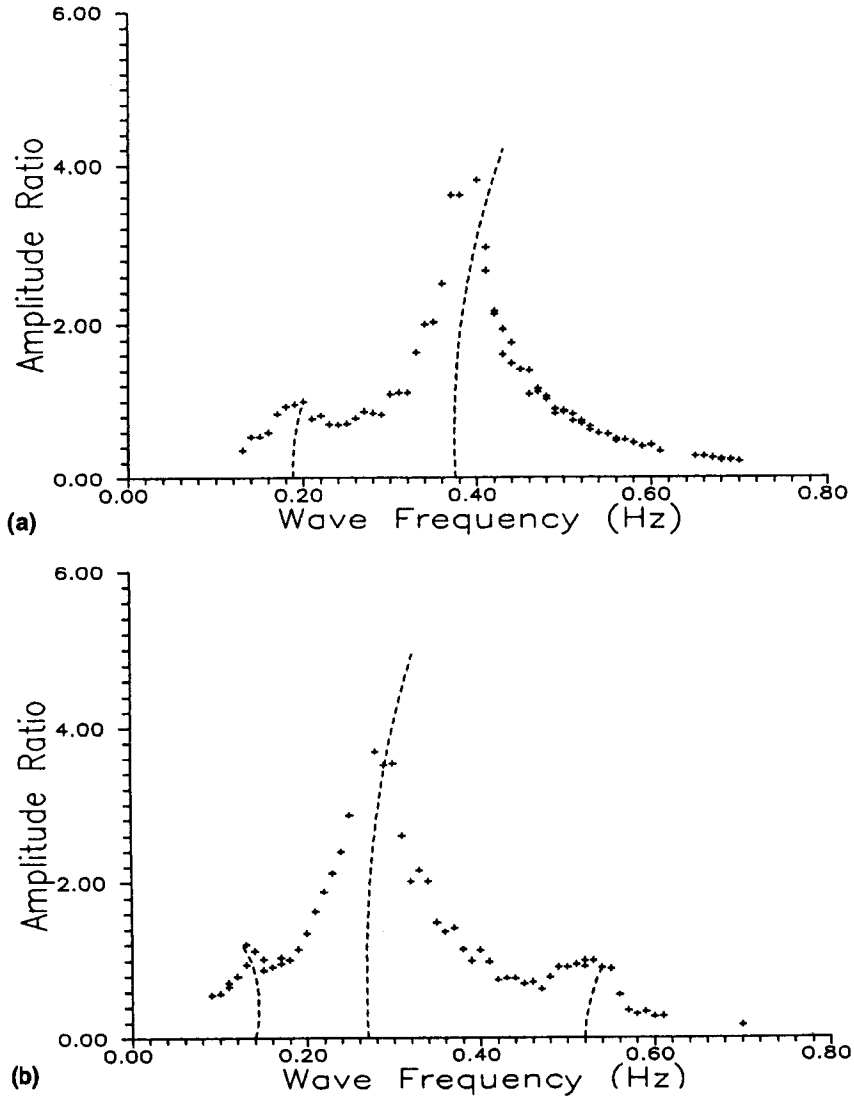

FIG. 2. Frequency Response Ratio (Response Amplitude/Wave Amplitude) versus Wave Frequency: (a) 60° Configuration; (b) 90° Configuration

It is shown that for the 60° configuration the primary resonance, $R_{1/1,1}$ (Gottlieb et al. 1997) is located near 0.4 Hz and the backbone curve tilts over to the right owing to its hardening stiffness. A secondary resonance, $R_{2/1,1}$, is also shown near 0.2 Hz; thus loss of response stability may be observed near the region. Based on the experimental search test observations, harmonic responses become unstable and transition to ultraharmonic within the frequency range of 0.17–0.25 Hz.

The relationship of sphere response and wave with the 90° configuration is shown in Fig. 2(b). Primary resonance is located near 0.27 Hz ($R_{1/1,1}$), and two secondary resonances are observed near 0.14 Hz ($R_{2/1,1}$) and 0.53 Hz ($R_{1/2,1}$), respectively. Note that the primary resonance tilts over to the right and the low frequency secondary resonance (0.14 Hz) leans over to the left, which agrees with the numerical result by Parlitz and Lauterborn (1985). Transitions between harmonic and ultraharmonic responses are observed near 0.11 and 0.16 Hz, and ultraharmonic response dominates the system behavior within the wave frequency range of 0.11–0.16 Hz. The loss of response stability near resonance regions is analytically predicted in Gottlieb et al. (1997). Period doublings are also observed in the experiment near the location of high frequency secondary resonance (0.53 Hz). Within the frequency range 0.46–0.56 Hz, period doubling bifurcations are frequently observed, and a signature of the superstructure is indicated to exist in the moored system.

Data Acquisition Tests

A set of data acquisition tests are conducted to obtain steady-state responses for each configuration (e.g., 60° and 90°).

Despite a lower degree of geometric nonlinearity, some ultraharmonic responses are observed for the 60° configuration. These ultraharmonic responses appeared strongly stable, reaching a steady state within a few cycles of the excitation and remaining in that state throughout the test. Because of its strong complex geometric nonlinearity, the model with 90° configuration exhibits the most interesting nonlinear responses as predicted. Both subharmonic (e.g., Fig. 3) and ultraharmonic response (e.g., Fig. 4) are frequently observed.

Experimental responses are compared to corresponding simulated solutions (using the estimated parameters) via time series [Figs. 3(b) and 4(b)] and energy spectra [Figs. 3(d) and 4(d)]. For both ultraharmonic (Fig. 3) and subharmonic (Fig. 4) responses, the numerical predicted motions provide good agreement in both response amplitude and phase shift in the time domain, and the analytical model is thus validated.

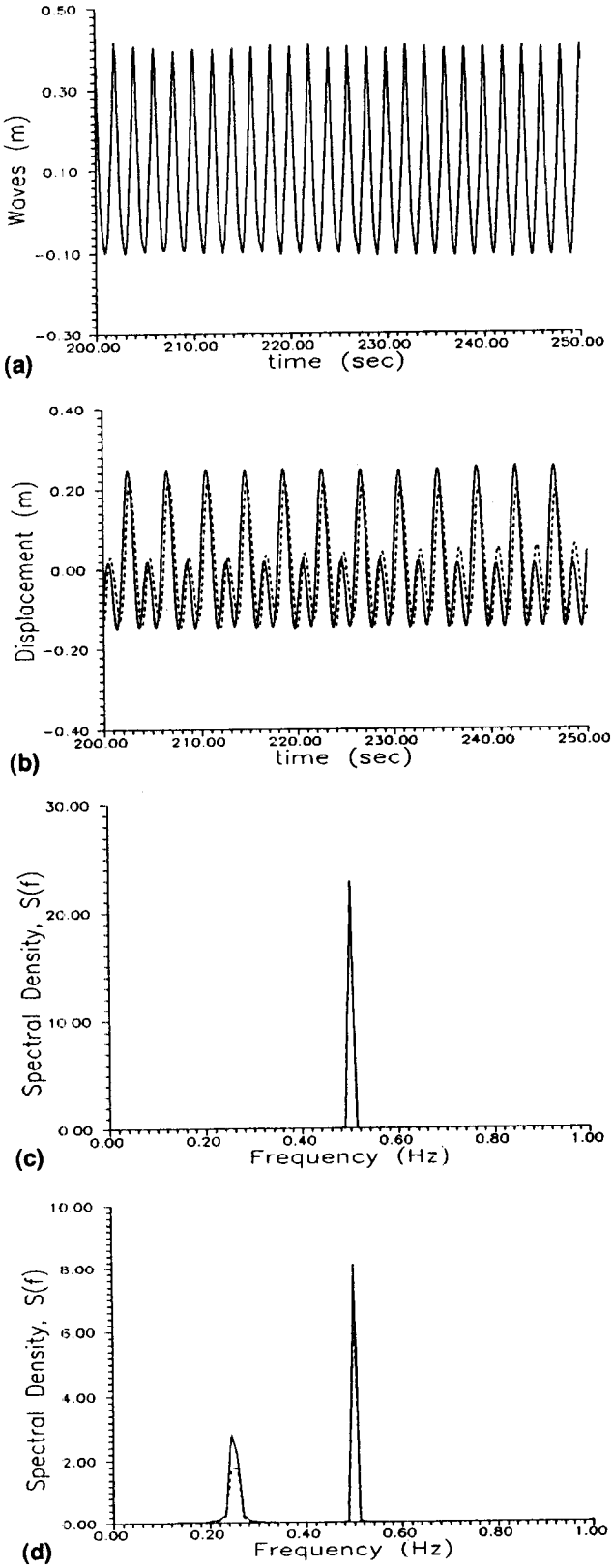

FIG. 3. Subharmonic Structural Response to Monochromatic Wave Excitation (Test D9—90° Configuration): (a) Wave Profile; (b) Response Time History (Measured = Solid Line; Simulated = Dashed Line); (c) Wave Spectral Density; (d) Response Spectral Density (Measured = Solid Line; Simulated = Dashed Line)

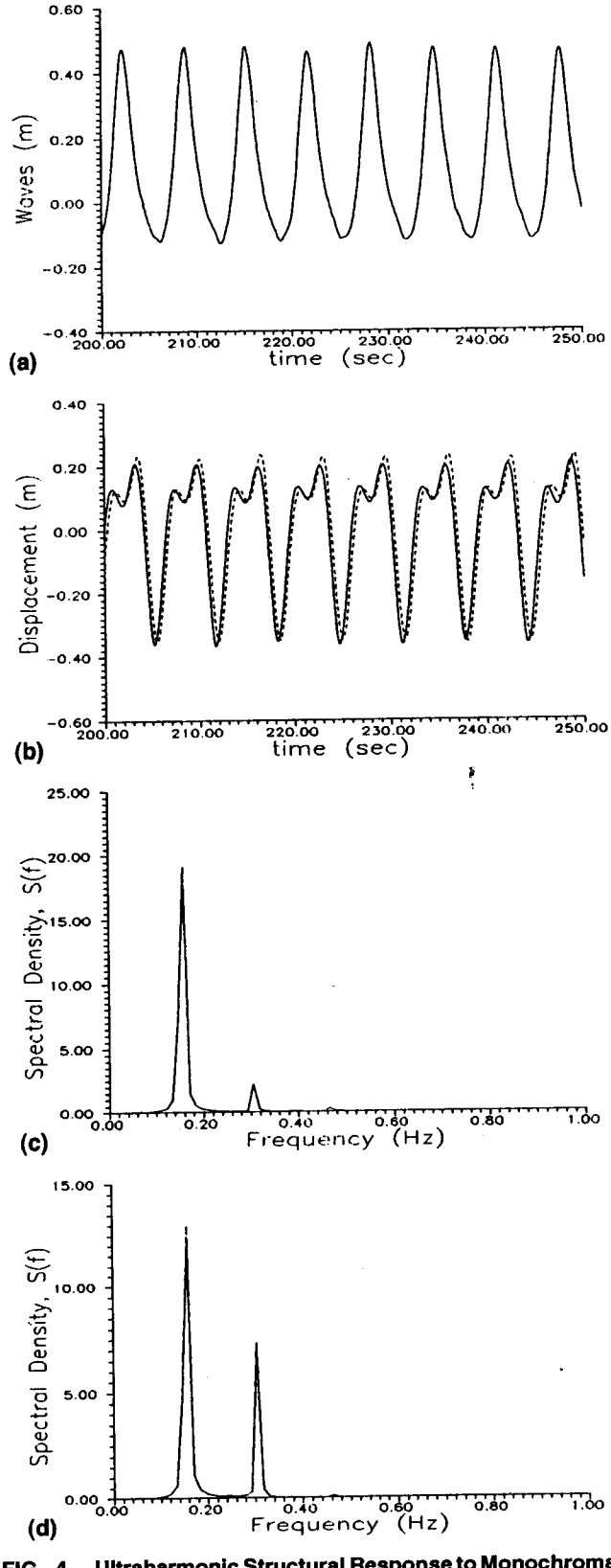

FIG. 4. Ultraharmonic Structural Response to Monochromatic Wave Excitation (Test D3—90° Configuration): (a) Wave Profile; (b) Response Time History (Measured = Solid Line; Simulated = Dashed Line); (c) Wave Spectral Density; (d) Response Spectral Density (Measured = Solid Line; Simulated = Dashed Line)

COMMENT

The existence of harmonic, subharmonic, and ultraharmonic responses in the experimental model clearly demonstrates the highly nonlinear nature of the moored system responses. The existence of underlying superstructure in bifurcations is indicated and inferred by the observed transitions (e.g., period doubling) between resonances. However, owing to physical limitations of the experimental model and laboratory facilities,

the relatively small number of tests conducted, and the restrictive quiescent initial condition for all tests, no obvious deterministic higher-order steady-state nonlinear responses (e.g., quasi-periodic and chaotic) are identified. In spite of these limitations, the experimental observations (especially Fig. 2), along with the analytical/numerical predictions, indicate that high-order nonlinear responses may reside in the transient portion or in the domain of attraction other than quiescent initial conditions.

ACKNOWLEDGMENT

The financial support from the United States Office of Naval Research Grant No. N00014-92-1221 is gratefully acknowledged.

APPENDIX. REFERENCES

Gottlieb, O., and Yim, S. C. S. (1992). "Nonlinear oscillations, bifurcations and chaos in a multi-point mooring system with a geometric nonlinearity." *Appl. Oc. Res.*, 14, 241–257.

Gottlieb, O., Yim, S. C. S., and Lin, H. (1997). "Analysis of bifurcated superstructure of nonlinear ocean system." *J. Engrg. Mech.*, ASCE, 123(11), 1180–1187.

Moon, F. C. (1987). *Chaotic vibrations*. John Wiley & Sons Inc., New York, N.Y.

Nayfeh, A. H., and Mook, D. T. (1979). *Nonlinear oscillations*. John Wiley & Sons Inc., New York, N.Y.

Parlitz, U., and Lauterborn, W. (1985). "Superstructure in the bifurcation set of the Duffing equation." *Phys. Letters A*, 107(8), 351–355.

Triantafyllou, M. S., and Yue, D. K. P. (1995). "Damping amplification in highly extensible hysteretic cables." *J. Sound and Vibration*, 186, 355–368.

Yim, S. C. S., Myrum, M. A., Gottlieb, O., Lin, H., and Shih, I.-M. (1993). "Summary and preliminary analysis of nonlinear oscillations in a submerged mooring system experiment." *Oc. Engrg. Rep. No. OE-93-03*, Oregon State University, Corvallis, Oreg.